Quantifying the Ozone Radiative Feedback on Planetary-Wave and Zonal-Mean Variability during the Southern Hemisphere Stratospheric Polar Vortex Breakdown

MERYL C. ANIL,[a] MICHAELA I. HEGGLIN,[a,b] THEODORE G. SHEPHERD,[a] INNA POLICHTCHOUK,[c] AND TIMOTHY N. STOCKDALE[c]

[a] *Department of Meteorology, University of Reading, Reading, United Kingdom*
[b] *Forschungszentrum Jülich, Institute of Climate and Energy Systems - Stratosphere, Jülich, Germany*
[c] *European Centre for Medium-Range Weather Forecasts, Reading, United Kingdom*

(Manuscript received 7 March 2024, in final form 26 November 2024, accepted 13 December 2024)

ABSTRACT: Stratospheric ozone has been shown to impact stratospheric variability and subseasonal-to-seasonal (S2S) prediction via its strong radiative properties. Previous research investigating the impact of interactive ozone in atmospheric models, compared with the use of a prescribed climatology, has focused largely on the zonal-mean impacts. Here, we employ a process-based diagnostic to quantify the impact of interactive ozone on high-latitude stratospheric variability in the Southern Hemisphere during the vortex breakdown period using two seasonal hindcast ensembles (one with and one without interactive ozone) initialized on 1 October over a period of 29 years. We focus on the amplitudes of waves (i.e., the longitudinal deviations from the zonal mean) and of zonal-mean deviations from the ensemble mean, for both temperatures and zonal winds. The effect is quantified as a function of day of year, considering the strong nonstationarity during this season, and we focus on the lower stratosphere, a region crucial for stratosphere–troposphere coupling. For both the waves and the zonal mean, we show that interactive ozone provides a positive radiative feedback on the variability. This increases the variances of both the waves and the zonal-mean deviations. Also, the ozone–temperature correlations are strengthened. The feedback acts most strongly on zonal wavenumbers 1 and 2. Interactive ozone is found to increase the predictable signal of the final warming date, bringing it closer to reanalysis, even though the anomaly correlation coefficient is reduced. This reflects the limitations of the anomaly correlation coefficient as a metric of skill in the presence of a signal deficit.

SIGNIFICANCE STATEMENT: The stratosphere is known to impact the troposphere during periods of high variability through stratosphere–troposphere coupling. This coupling has been shown to impact weather prediction on the subseasonal-to-seasonal (S2S) time scales (2 weeks to a season), important for decision-making in sectors including water, food, and energy. Our study analyzes the importance of stratospheric ozone, specifically its radiative feedback, in impacting the stratospheric variability (focusing on the variability of temperature and zonal winds) on S2S time scales by comparing model results that include and omit this feedback. We show that the ozone radiative feedback increases both temperature and zonal wind variability and thus increases the range of possibilities explored by the model, which can potentially lead to impacts on S2S prediction.

KEYWORDS: Southern Hemisphere; Planetary waves; Internal variability; Seasonal variability; Ozone

1. Introduction

Stratospheric ozone variability has been shown to have impacts on tropospheric weather on subseasonal-to-seasonal (S2S) time scales, especially in the Southern Hemisphere (SH) due to the presence of the ozone hole providing a strong radiative signal (McLandress et al. 2011; Polvani et al. 2011; Kang et al. 2011; Son et al. 2013). These studies reveal a strong negative correlation between spring polar ozone concentrations and the summer Southern Annular Mode (SAM) index, which modulates the spatial distribution of precipitation and temperature in the SH troposphere (Thompson and Wallace 2000; Fogt and Marshall 2020). In the case of long-term changes induced by the development of the ozone hole, the causal chain is that polar ozone depletion leads to a stronger polar vortex via ozone radiative impacts, which via reduced poleward transport of ozone leads to an even stronger polar vortex, a delayed vortex breakdown, and a delayed equatorward shift of the midlatitude jet (Randel and Wu 1999; Byrne et al. 2017). Stratospheric ozone can also be expected to play a role in the internal, year-to-year variability in the SH polar lower stratosphere (Salby et al. 2012). The causal chain is the same as for the long-term changes induced by polar ozone depletion, except that it is set off by year-to-year dynamical variability rather than by polar ozone depletion. The final step in the chain, namely, the stratosphere–troposphere coupling between the strength of the polar vortex and the SAM, is the same for year-to-year variability as for the long-term changes (Saggioro and Shepherd 2019). The comparatively long time scales of stratospheric polar variability can then provide a source of predictability for tropospheric

Denotes content that is immediately available upon publication as open access.

Corresponding author: Meryl C. Anil, m.chittethazhathuanil@pgr.reading.ac.uk

DOI: 10.1175/JAS-D-24-0045.1

weather (Byrne et al. 2019; Lim et al. 2021), analogous to what is seen for the Northern Hemisphere (NH) (Baldwin and Dunkerton 2001). Such predictability does not depend on the representation of ozone in models but can be expected to be affected by it.

Whether the radiative feedbacks of stratospheric ozone have significant enough impacts on the troposphere to be worth the cost of inclusion in numerical weather prediction (NWP) models has been an active topic of research (e.g., Bergner et al. 2022). The answer will necessarily depend on the forecast time scale. The representation of ozone in NWP models currently ranges from prescribing a two-dimensional zonal-mean monthly mean climatology in the radiation scheme, to a three-dimensional climatology, to the use of fully interactive ozone, where the radiation scheme sees the prognostic ozone field generated by an ozone parameterization scheme. This is to be contrasted with state-of-the-art chemistry–climate models (CCMs), which include a physically based and fully interactive stratospheric chemistry scheme (Young et al. 2018). Interactive ozone allows the entire ozone feedback loop to be represented in the model, i.e., the chemistry (ozone) can affect dynamics and be affected by it, whereas prescribing any form of climatology breaks the feedback loop. It is important to distinguish between the effects of interactive ozone and the effects of a more realistic ozone climatology, e.g., one including zonal asymmetries, as the latter can itself affect the stratospheric mean state and hence stratospheric variability (Gillett et al. 2009; Haase and Matthes 2019; Rae et al. 2019).

That a realistically varying stratospheric ozone can improve the predictability of SH tropospheric weather is supported by the study of Hendon et al. (2020), who showed that prescribing the observed monthly mean ozone values in the 2002 SH stratospheric sudden warming (SSW) resulted in more realistic surface conditions compared to using a monthly mean climatology. Oh et al. (2022) extended this result by using yearly varying, monthly and zonally averaged ozone, showing an increase in skill in the troposphere with the more realistic ozone. Jucker and Goyal (2022) identified a potential mechanism for this effect based on a case study of the 2019 SH polar vortex weakening. However, in a forecast setting, the future ozone is not known and must be modeled, hence the need for interactive ozone in this context.

Several studies have shown that interactive ozone leads to an increase in NH stratospheric variability, resulting in a more realistic distribution of SSWs (Haase and Matthes 2019), strengthened strong polar vortex events (Oehrlein et al. 2020), an increase in temperature variability in the NH polar regions (Albers et al. 2013; Rieder et al. 2019), and increased variability in the timing of the NH final warming date (FWD) (Friedel et al. 2022). Tropical temperature variability was also shown to be enhanced (Yook et al. 2020). While there has been some research into the impacts of interactive ozone on planetary waves, e.g., Nathan and Cordero (2007) and Silverman et al. (2018) for the NH, the focus of most studies has largely been on the feedbacks on the zonal-mean variability resulting from including interactive ozone. We can also expect that the details of the impact of interactive ozone on polar variability will be different in the SH compared to the NH polar regions, because of the different dynamical regimes in the two regions.

This paper aims to add to the existing literature by using an operational forecast model to quantify the strength of the ozone radiative feedback in a process-oriented manner and the extent to which interactive ozone acts to amplify or dampen variability on S2S time scales, with an emphasis on planetary waves, as well as zonal-mean variability. The focus is on the polar lower stratosphere during the SH final warming period when stratosphere–troposphere coupling is strongest (Gerber et al. 2010). Although low polar temperatures can be expected to be associated with low polar ozone in the lower stratosphere in the zonal mean, it is not self-evident that such a strong positive correlation can be expected for waves due to the different time scales on which ozone and temperature anomalies are built up through advection (Randel 1993; Nathan and Cordero 2007). We focus on the variability rather than the mean state of the stratosphere because that is where interactive ozone is expected to have the most impact. Moreover, the mean state in a model will inevitably reflect the effects of many competing processes, such that there is no direct relationship between improvements in a single process (e.g., the radiative impact of ozone) and improvement in the overall mean state. Importantly, the large sample size of our experiments allows us to quantify the effects of interactive ozone as a function of day of year, which is important given the strong nonstationarity of the stratosphere during this time of year. We also briefly explore how interactive ozone affects the prediction of the FWD.

The remainder of the paper starts with describing the dataset and analysis methods in section 2. The latter includes the definition of the effective feedback parameter which is the metric used to quantify the ozone radiative feedback. The results are described in section 3. First, the impacts on the zonal-mean variability are quantified in section 3a followed by an investigation into planetary-wave variability in section 3b. The results section concludes with section 3c which focuses on the impacts during the vortex breakdown period, including the predictability of the FWD. The paper concludes with a summary and discussion in section 4.

2. Data and methods

a. Data

The analysis was conducted on a set of ensemble hindcasts generated using the European Centre for Medium-Range Weather Forecasts (ECMWF) Integrated Forecasting System (IFS) model, specifically cycle 47R1 at Tco199 (about 57-km grid spacing) horizontal resolution (ECMWF 2020). This cycle included 137 vertical levels from the surface to 0.01 hPa (roughly 80 km), as is used for ECMWF's operational weather prediction today, and was coupled to the 1° Nucleus for European Modeling of the Ocean (NEMO) ocean model with sea ice modeled with the prognostic LIM2 model, which is part of the NEMO modeling framework. It should be noted that this version of the IFS was not tuned with interactive ozone.

The 15-member ensemble hindcasts were initialized on 1 October using the fifth major global reanalysis produced by ECMWF (ERA5) data for each year spanning 1992–2020, followed by a free-running simulation for 4 months. The ensemble was generated by making small perturbations to the initial conditions. Two separate hindcasts were constructed, sharing identical characteristics except for their treatment of ozone in the radiation scheme. In the first ensemble [control (CTRL)], a 2D ozone climatology was introduced which is interpolated from zonal-mean monthly mean fields derived from the Copernicus Atmosphere Monitoring Service (CAMS) reanalysis. In the second ensemble [radiatively interactive (RADINT)], the model's prognostic ozone is utilized. Thus, pairs of ensemble members in RADINT and CTRL start from the same initial condition but will diverge because of the differences in radiative tendencies. It is important to distinguish between the random differences which result from chaos and are just triggered by interactive ozone and the systematic differences which are causally attributable to interactive ozone, which we can do because of the large sample size produced by the hindcast ensembles. Both ensembles have prognostic ozone using the Hybrid Linear Ozone (HLO) scheme, which is a linear ozone parameterization scheme similar to the well-known Cariolle–Déqué (CD) scheme (Cariolle and Déqué 1986) and which is now operational in the IFS. Therefore, the two prognostic ozone fields can be compared. The HLO scheme is successful in providing an accurate synoptic evolution of ozone, especially compared to fixed zonal-mean profiles that would otherwise be used. Thus, it is fully suited to the purposes of this study. Full documentation of the HLO scheme has not yet been published, so we have provided some technical details and its suitability for our experiment in the appendix.

Although both RADINT and CTRL generate a prognostic ozone field using the HLO scheme, in CTRL the prognostic ozone is just a diagnostic whereas in RADINT it impacts the meteorology via radiation. Therefore, when comparing the ozone fields between the two sets of experiments, they should exhibit similar statistical distributions, with the robust differences attributable to the ozone radiative feedback. It should be noted that since the ozone climatology used by the radiation in CTRL is derived from CAMS analyses, and not from the corresponding RADINT experiment, the climatology of ozone seen by the radiation in the two experiments is different. The ozone climatology seen by CTRL generally shows a lower ozone compared to the climatology produced by HLO. There are multiple possible reasons for this [e.g., different time periods between the HLO training years and years used to derive the CAMS climatology (see the appendix), biases in model temperatures and/or transports, nonlinearities in the ozone behavior, rectification effects from the radiative interaction], and detailed investigations would be outside the scope of our paper. Our analyses focus on anomalies relative to zonal means or ensemble means and so to first order are insensitive to any difference in the overall absolute mean climatology. Nonetheless, the difference in mean climatology seen by the radiation in CTRL and RADINT could conceivably contribute to slight differences in some of our statistics, which might lead to a slight overestimation of our quantitative estimates for the impact of interactive ozone. Given the nature of our analyses, however, we consider our overall conclusions to be robust.

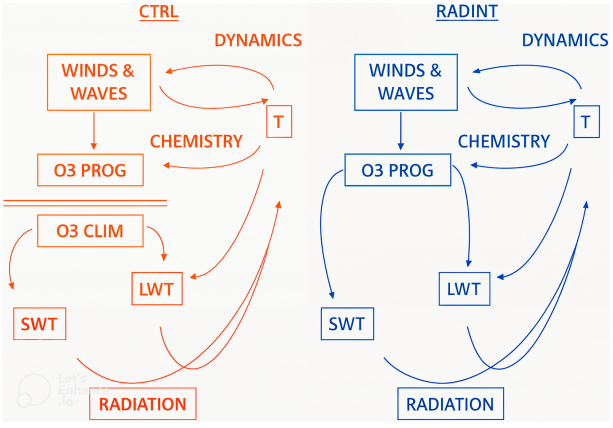

FIG. 1. Radiative, chemical, and dynamical feedbacks involving ozone in the lower stratosphere shown for both a prescribed ozone climatology (CTRL) and an interactive ozone (RADINT). The feedback loop is complete in RADINT but is disrupted when using an ozone climatology in CTRL.

Finally, we use the ERA5 data for forecast skill analysis.

b. *Methods*

We focus on the SH, due to 1) the ozone hole being present at the start of the experiment and therefore providing a strong signal of interannual ozone variability and 2) the simulation period encompassing the final warming and vortex breakdown in the SH, which is when planetary-wave activity is particularly enhanced. As mentioned in section 1, the focus is on the lower stratosphere due to 1) its importance to stratosphere–troposphere coupling and 2) the presence of the ozone hole in this region. Since there is a strong seasonal cycle present during these months, all the analysis is conducted as a function of day of year. The first 2 weeks are ignored as spinup.

As mentioned in section 1, the ozone feedback loop involves chemistry, radiation, and dynamics, as shown in Fig. 1. The physically realistic RADINT loop shows the two-way feedback between ozone and dynamics via radiation and chemistry: Ozone affects temperature through its radiative impacts, which then affects dynamics and chemistry, which subsequently impact ozone. In CTRL, this feedback loop is broken. Here, we focus on quantifying the first step in the feedback of ozone on the system, namely, the effect of shortwave tendency (SWT) and longwave tendency (LWT) on temperature. We investigate the impact of interactive ozone on 1) the zonal-mean variability, i.e., deviations away from the ensemble mean using data grouped across all years, and 2) the waves, i.e., the deviations away from the zonal mean, using data grouped across all years and all ensemble members. For item 1, this choice avoids the potentially confounding influence of interannual variability, so as to focus on the model spread for a given year. We quantify the impact on waves at 60°S because this latitude is generally close to the edge of the polar vortex, and thus, wave activity here is

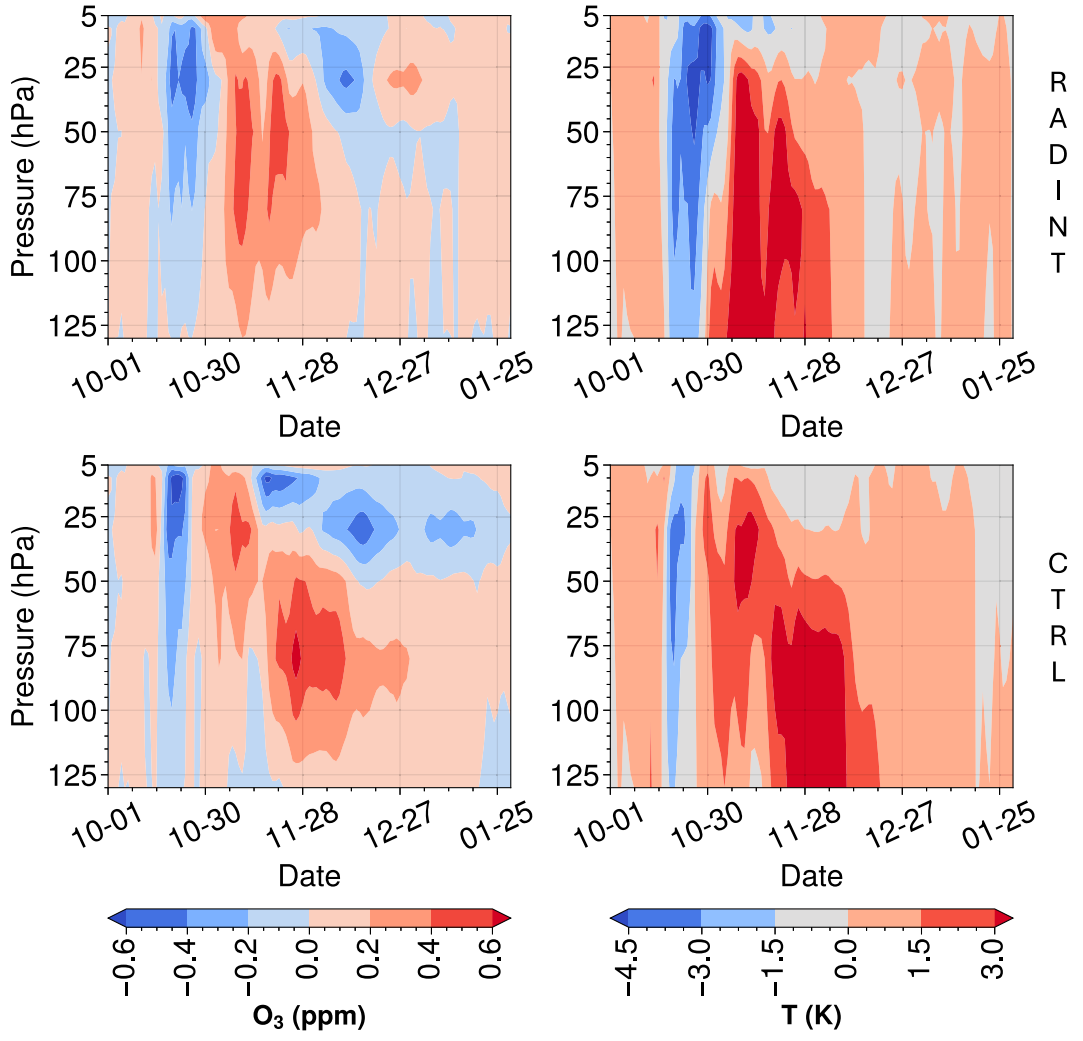

FIG. 2. Polar cap (60°–90°S) evolution of (left) ozone (ppm) and (right) temperature (K) deviations from the ensemble mean for a single year (2018) and a single ensemble member (member 0) for (top) RADINT and (bottom) CTRL to illustrate the positive correlation between the ozone and temperature anomalies which arises from dynamical variability.

important for disturbing the vortex. For the variations in the zonal mean, we quantify the impact at 60°S for the zonal-mean wind and the average over the polar cap from 60° to 90°S for ozone and temperature. This is consistent with how zonal-mean stratospheric polar vortex variability is generally represented and reflects thermal wind balance. For the same reason, the zonal wind variability is quantified at 50 hPa while the ozone and temperature variability are quantified at 80 hPa, although we also briefly examine higher altitudes as well.

In addition to standard statistical measures such as correlations and variances, we also introduce the effective feedback parameter (EFP) to quantify the radiative feedback of both SWT and LWT on temperature T. Mathematically, the EFP is derived from the temperature tendency equation as follows:

$$\frac{\partial T'}{\partial t} = \mathrm{SWT}' + \mathrm{LWT}' + (\text{other processes}). \tag{1}$$

Here, the primes indicate spatial deviations, either from the zonal mean for the waves or from the ensemble mean for the zonal mean. Given our focus is on the lower stratosphere where the diurnal cycle is weak, daily averages are used for temperature and ozone, while radiative tendencies are presented as daily accumulations. However, it should be noted that the strong diurnal cycle in the upper stratosphere could be sensitive to these measures. Ignoring the other processes in Eq. (1) and focusing on the effects of SWT, multiplying through by T' and averaging (either over longitudes or over ensemble members, as appropriate, and denoted by an overbar) results in

$$\frac{1}{2}\frac{\partial}{\partial t}(\overline{T'^2}) = \overline{T'\frac{\partial T'}{\partial t}} = \overline{T'\mathrm{SWT}'}. \tag{2}$$

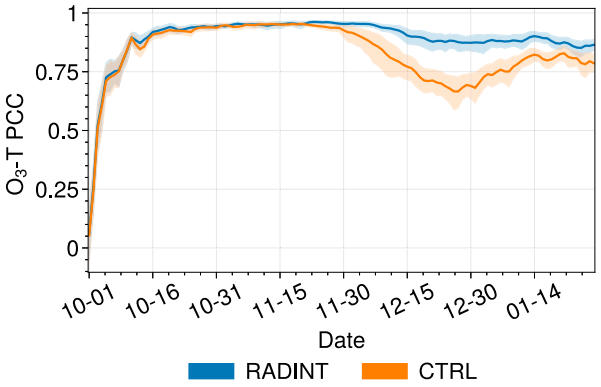

FIG. 3. PCC between polar cap ozone and temperature deviations from the ensemble mean, across all years, for RADINT (blue) and CTRL (orange). The figure is produced using latitudes 60°–90°S and the 80-hPa pressure level. The shading shows the 95% confidence interval around the bold lines which indicate the multiyear mean.

Dividing Eq. (2) by $\overline{T'^2}$, i.e., the variance of temperature, results in

$$\frac{1}{2}\frac{\partial}{\partial t}(\log \overline{T'^2}) = \frac{\overline{T'\mathrm{SWT}'}}{\overline{T'^2}}. \tag{3}$$

Equation (3) represents a feedback equation: If the right-hand side is positive, then the SWT acts as a positive feedback on the variance. We can thus define the EFP as follows:

$$\mathrm{EFP} = \frac{\overline{T'\mathrm{SWT}'}}{\overline{T'^2}}. \tag{4}$$

The EFP has units of inverse time and is defined for each year and each day of the year, and in the case of the waves, also for each ensemble member. It is equivalent to the covariance of SWT and T divided by the variance of T. A similar diagnostic is widely used in tidal theory to represent the damping of the atmospheric thermal tide by wave drag (McLandress 2002). An alternative way of interpreting the EFP is that it is the linear regression coefficient of SWT against T and therefore represents what the radiation code is doing if it were approximated by a linear term (Hitchcock et al. 2010). LWT is treated analogously. The two terms can be added to obtain the net radiative feedback. Furthermore, using spectral decomposition, the contributions to the EFP from different wavenumbers of SWT and T can also be isolated.

3. Results

a. *Zonal mean (lower stratosphere)*

First, the impact of the ozone radiative feedback on the zonal mean/polar cap is examined as this has been the focus of previous studies, as discussed in section 1. For that, we examine the zonal-mean deviations from the ensemble mean for each year, so as not to conflate this aleatoric variability with the predictable variability from year to year. The weighted

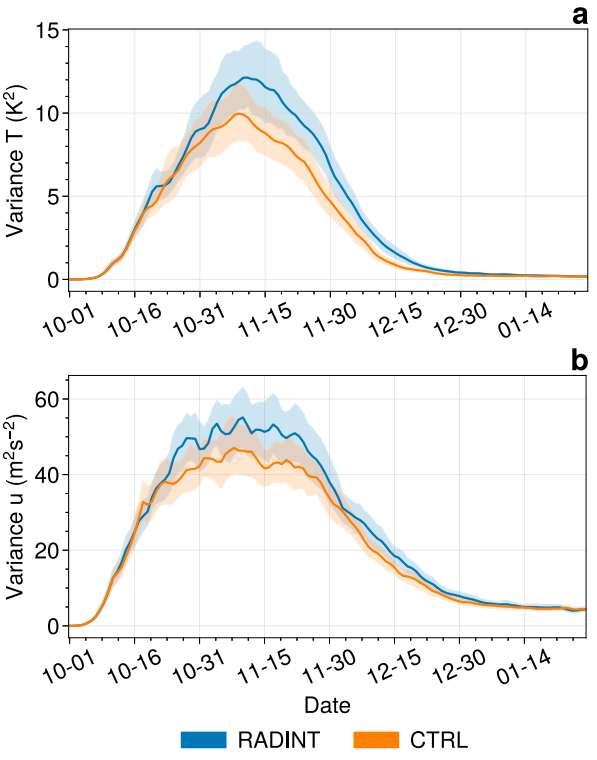

FIG. 4. The polar cap temperature (K^2) and zonal-mean zonal wind ($m^2\ s^{-2}$) variance with respect to the ensemble mean for RADINT (blue) and CTRL (orange). The polar cap average temperature is calculated using latitudes 60°–90°S at 80 hPa, and the zonal wind is calculated at 60°S and 50 hPa.

polar cap average south of 60°S is used for temperature, prognostic ozone, SWT, and LWT, as a robust measure of zonal-mean variability. These are all analyzed in detail at 80 hPa. Zonal wind is instead calculated at 60°S and 50 hPa, consistent with thermal wind balance. To provide a physical motivation for the quantitative analysis, Fig. 2 shows a snapshot of the seasonal evolution of temperature and ozone polar cap deviations for ensemble member 0 in 2018 for pressure levels 5–130 hPa and is merely intended to be illustrative. We see a strong positive correlation between temperature and ozone for both RADINT and CTRL, with the pattern reflecting the well-known downward propagation of zonal-mean polar vortex anomalies (Byrne and Shepherd 2018). The question is whether this correlation, which is dynamical in origin, is strengthened by interactive ozone. To address this, the Pearson correlation coefficient (PCC) between the ozone and temperature is shown in Fig. 3 as a function of day of year, across all years using 95% confidence intervals calculated using bootstrapping (based on resampling with replacement 1000 times). There is an initial spinup period while the zonal means of the ensemble members begin to separate. Following that spinup period, the correlations are very high in both ensembles, but starting in late November, the correlations in CTRL start to decline, whereas they remain high in RADINT and continue to be higher than CTRL even as the CTRL correlations recover somewhat in

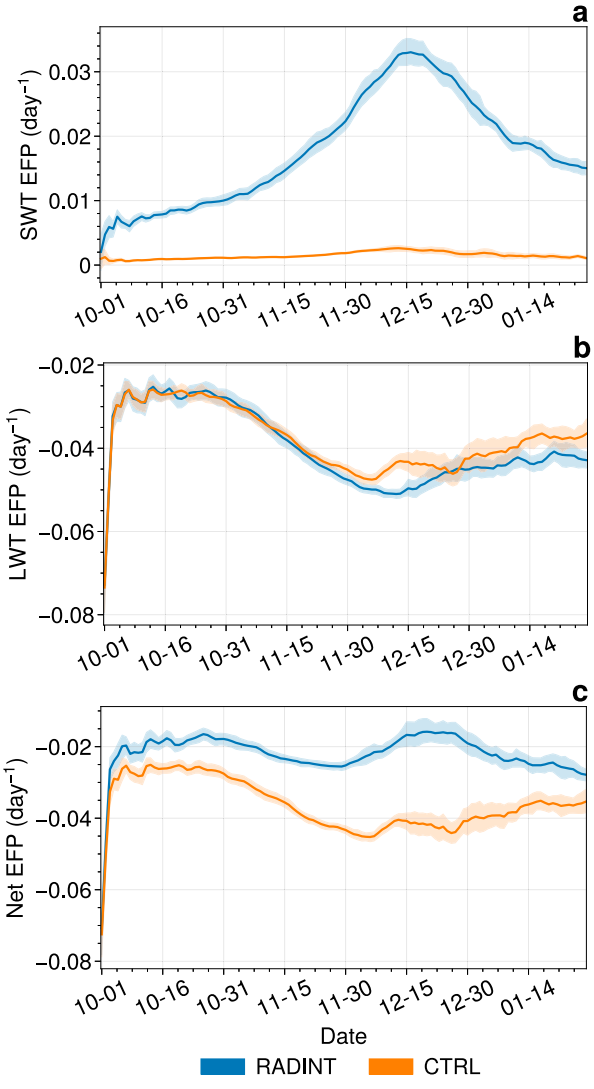

FIG. 5. The EFP for (a) SWT, (b) LWT, and (c) their sum (Net) all in units of per day, for zonal-mean deviations away from the ensemble mean, for RADINT (blue) and CTRL (orange). This is calculated using latitudes 60°–90°S and 80 hPa.

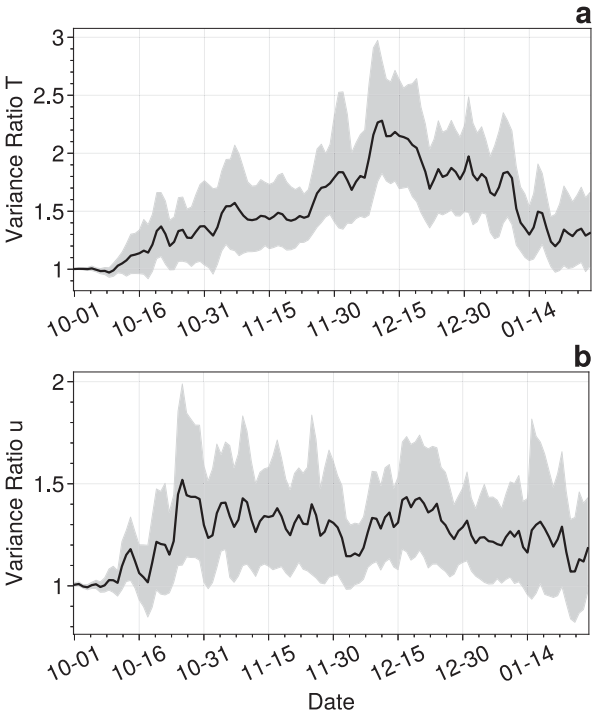

FIG. 6. Ratio of the variances in (a) 80-hPa polar cap temperature and (b) 60°S zonal-mean zonal wind between RADINT and CTRL.

early January due to the transition into the calmer summer stratosphere. A similarly evolving pattern is observed for the correlation between SWT and T for RADINT, i.e., high positive values with a reduction around the final warming date averaging around 0.72 across the entire period, while CTRL averages to zero as expected. The differences for the LWT correlation are less pronounced between RADINT and CTRL, averaging around −0.86 and −0.83, respectively (not shown).

The higher PCC values in RADINT indicate that the ozone–temperature correlation in the zonal mean is strengthened by the ozone feedback. We would then expect strengthened temperature variability as well, due to the variable ozone in RADINT, which is indeed seen in Fig. 4. This is consistent with previous research, including Monge-Sanz et al. (2022), whose Fig. 17 shows a similar effect to that in Fig. 4a, albeit for a slightly different statistic of polar cap variability. In our S2S setup, it takes time for the variances (which reflect the ensemble spread) to grow because the initial perturbations are so small, and they decline as the vortex weakens. The PCC values in Fig. 3 do not show such behavior because they represent a normalized statistic. As the variances grow, the differences between RADINT and CTRL become apparent.

While the correlation between the radiative tendencies and temperature measures the linear relationship between the two variables, the strength of the radiative feedback is investigated by calculating the SWT and LWT EFPs. The EFPs for the zonal-mean anomalies are shown in Fig. 5a where CTRL SWT EFP is seen to be almost zero (since the radiation code sees the same climatological ozone field for all ensemble members), while RADINT shows clear positive values peaking just above 0.03 day^{-1}. The peak occurs close to the summer solstice when solar insolation is maximal. To put that value in context, Fig. 5b shows the LWT EFP and Fig. 5c the total EFP. The LWT EFP is very similar for both RADINT and CTRL, because it is mainly sensitive to temperature, and is negative reflecting the longwave cooling with a comparatively weaker seasonal dependence. The SWT EFP for RADINT is numerically smaller than the LWT EFP, but of a comparable magnitude, to the extent that the total EFP, which reflects the net radiative damping, is roughly halved in RADINT by the effect of interactive ozone. This is a nontrivial effect and accounts for the stronger variances in RADINT than in CTRL. The

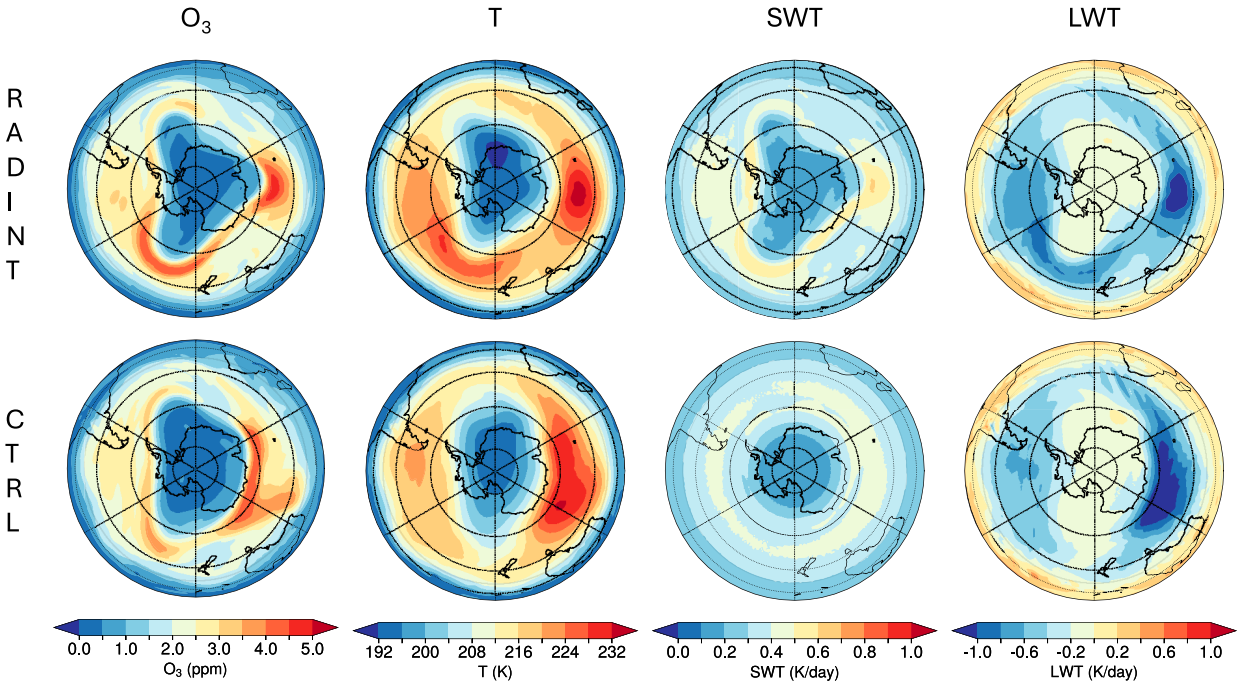

FIG. 7. Contour plots of (left to right) ozone (ppm), temperature (K), SWT (K day^{-1}), and LWT (K day^{-1}) on day 15 of the experiment for ensemble member 0 in 2018 for (top) RADINT and (bottom) CTRL. The plots are generated at 80 hPa.

RADINT values found here are broadly consistent with those found in Hitchcock et al. (2010) using a comprehensive chemistry–climate model, with a SWT EFP for the SH polar lower stratosphere of about 0.02 day^{-1} averaged over December (their Fig. 9a) and a total EFP of about -0.02 day^{-1} over spring and summer (their Figs. 10a,d), noting that in Hitchcock et al. (2010), there is a reversal in sign compared to our results because they report damping rather than feedback parameters.

Since the ozone radiative feedback is an amplifying feedback, it should be more clearly manifest in the ratio of the variances between RADINT and CTRL, which are shown in Fig. 6, rather than in their absolute differences. Although the ratio is a noisy statistic, the temperature variance ratio (Fig. 6a) does broadly peak around the same date as the SWT EFP, at a value of around 2. An exact match in timing is not expected since it takes time for the radiative tendency to affect the temperature, and the variance also depends on the dynamical processes driving it, which will have a seasonal dependence. The importance of these other processes is apparent in the ratio of zonal wind variances (Fig. 6b), whose seasonal evolution is less clearly linked to that of the SWT EFP and indicates a roughly 30% increase in variance from interactive ozone throughout the vortex breakdown period.

b. *Waves*

1) LOWER STRATOSPHERE

We now turn our attention to the impacts of interactive ozone on waves (deviations from the zonal mean). To provide some physical intuition in this case, contour plots of 80-hPa ozone, temperature, SWT, and LWT are shown in Fig. 7. They are snapshots for a single ensemble member (ensemble member 0 as used in Fig. 2) for a given year (2018) on day 15 of the experiment and are merely intended to be illustrative. Day 15 gives enough time for significant divergence to arise between the two simulations. What is clear is that ozone and temperature are strongly positively correlated in both simulations, reflecting the fact that dynamics, in the form of horizontal advection, is the primary driver of the ozone wave variability. This is analogous to what was observed in section 3a, but in that case, the variability was in the zonal mean. The differences between RADINT and CTRL in Fig. 7 are clearly seen in the SWT, where RADINT closely follows the zonally asymmetric wave-3 ozone pattern shown, which is expected since the radiation code sees this prognostic ozone field. In contrast, CTRL shows a more zonally symmetric SWT resulting from the 2D monthly mean zonal-mean ozone climatology fed into the radiation scheme. There are small deviations from zonal symmetry in the SWT field in CTRL which presumably represent albedo effects. The LWT is shown to follow the spatial pattern of temperature in both simulations, with regions of high temperature corresponding well to regions of strong longwave cooling, as expected. There is perhaps a hint of stronger wave amplitudes in the RADINT temperature field, but this is only a snapshot, and we quantify this rigorously further below.

First, analogous to Fig. 3, the PCC between ozone and temperature is calculated, except here for zonally varying quantities. Figures 8a and 8b show using boxplots that for both RADINT and CTRL, the PCC values are high on average,

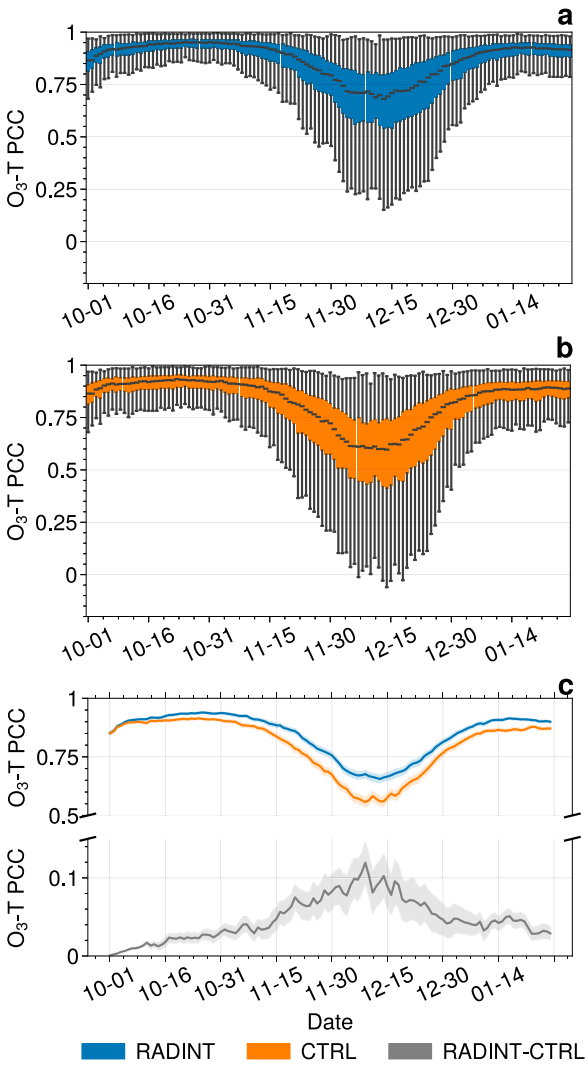

FIG. 8. (a)–(c) PCC between ozone and temperature deviations from the zonal mean for RADINT (blue) and CTRL (orange). The figure is generated at 60°S and 80 hPa. In (a) and (b), the shading shows the IQR, and the whiskers indicate the farthest data point within 1.5 times the IQR from the nearest hinge. In (c), the shading shows the 95% confidence interval about the bold lines which indicate the mean values, and the gray line (with expanded vertical scale) shows the difference between RADINT and CTRL.

although CTRL shows a larger spread with occasional values dropping to a negative correlation. This correlation in both experiments can be explained as being due to the presence of the strong polar vortex in the SH winter, isolating the air within it, which leads to a correlation due to horizontal equatorward (poleward) advection of cold (warm) air masses low (high) in ozone as seen in Fig. 7. Both RADINT and CTRL are seen to dip to lower PCC values around late November. This can be attributed to the seasonal variability observed in the stratosphere nearing the final warming period which occurs around late spring/early summer. In particular, the breakdown of the polar vortex disrupts the planetary-wave structures of ozone and temperature that give rise to their high correlations. This hypothesis is supported by the fact that the PCC values for both RADINT and CTRL rise back up after the final warming period when the calmer summer stratosphere is fully established with more synoptic wave structures. Fig. 9 shows snapshots of ozone and temperature during the more chaotic final warming period (day 60) and during the calmer summer stratosphere (day 119), for comparison with Fig. 7. Although RADINT consistently shows higher PCC values than CTRL, it is during the final warming period that this difference becomes most pronounced. The differences are more clearly seen in Fig. 8c, which shows the same relationship together with 95% confidence intervals, which due to the larger sample size (15 PCC values per year) have much smaller uncertainties compared with the uncertainties in section 3a for the zonal-mean variability (1 PCC value per year). We can thus conclude that the ozone feedback strengthens the correlation between ozone waves and temperature waves, as it does between their zonal-mean deviations.

To further investigate the seasonality of the correlations seen in Fig. 8, the evolution of temperature variance, zonal wind variance, and zonal-mean wind is shown in Fig. 10. Temperature variance is used to measure the strength of the wave disturbances at 80 hPa while the winds are analyzed at 50 hPa, as before. Figure 10 shows that the temperature variance is larger in RADINT than in CTRL, and similarly for the variance of the zonal wind. The enhancement of the wave variances in RADINT emerges earlier than it does for the zonal-mean variances (Fig. 4). That the enhancement results from the direct effect of the interactive ozone on the waves, rather than indirectly from differences in the zonal-mean flow, is clear since the average zonal-mean zonal wind is very similar between RADINT and CTRL (Fig. 10c). We do not draw any conclusions from the similarity of the zonal-mean zonal wind climatology between RADINT and CTRL, but note that it simplifies our interpretation of the differences in variances.

The EFPs for SWT and LWT on temperature waves are shown in Fig. 11. The sign of the EFP is the same as the sign of the correlation between temperature and the radiative tendency, thus as already seen in Fig. 8, is positive for the SWT (in RADINT) and negative for the LWT (in both RADINT and CTRL). We show the SWT EFP for CTRL for completeness but do not discuss it since its effect is very small and is unrelated to the ozone radiative feedback. The SWT EFP in RADINT reaches values exceeding 0.01 day^{-1}, peaking in late November. The decay of the SWT EFP before the summer solstice is presumably associated with the reduced correlation between ozone and temperature waves as the vortex breaks up (see previous discussion concerning Fig. 8).

The values of the SWT EFP for the waves (Fig. 11a) are smaller than those for the zonal-mean variability (Fig. 5a). Since the LWT EFP is of a similar magnitude for the waves and for the zonal-mean variability for both RADINT and CTRL, this means that the net EFP for the waves is less affected by interactive ozone than it is for the zonal mean, being reduced by around 30% (Fig. 11c) rather than by a factor of 2 (Fig. 5c). Nevertheless, it remains the case that interactive ozone reduces the net radiative damping of the waves,

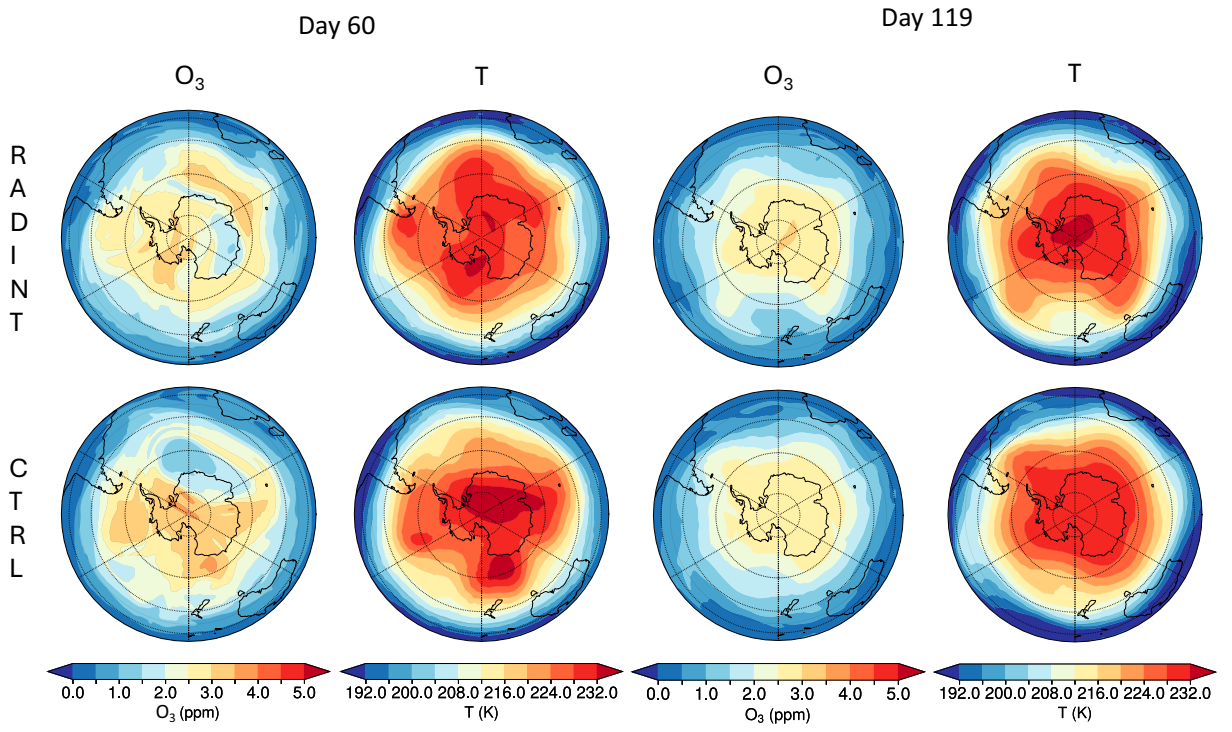

FIG. 9. As in Fig. 7, but for day 60 and day 119 of the experiment, showing contour plots of ozone and temperature at 80 hPa.

which can account for the larger wave variances. An analysis of the temperature variance ratios between RADINT and CTRL (not shown), analogous to Fig. 6, shows that as for the zonal-mean temperature variances, the magnitude of the ratio peaks close to the peak SWT EFP date.

Interestingly, there is already a difference between the LWT EFP in CTRL and RADINT at the beginning of the simulations, suggesting that ozone also plays a role in the longwave radiation. However, the differences are overall quite small, and a detailed investigation lies outside the scope of this paper, which is focused on the much larger effect on the SWT.

Using spectral decomposition, the impact of interactive ozone on different wavenumbers is shown in Fig. 12. The SWT EFP reaches a maximum for the more spatially coherent wavenumber 1 that is higher than the total SWT EFP shown in Fig. 11, indicating that at its maximum the ozone radiative feedback is stronger for wavenumber 1 than for the waves as a whole. There is also a distinct signature, albeit weaker, for wavenumber 2.

2) MULTILEVEL ANALYSIS

This section contains a brief analysis of the impact of interactive ozone on waves at other stratospheric altitudes. Figure 13 shows the correlations and EFPs for the waves for multiple levels. Here, only the mean values of each statistic are used for the contour plot. The levels used are 5, 10, 30, 50, 80, and 130 hPa.

First, the choice of 80 hPa is seen to be representative of the lower stratosphere as judged by the ozone–temperature PCC. It can also be seen that there is a downward propagation of the PCC values from around 10 hPa toward 130 hPa as time goes on, similar to the downward propagation of the zonal-mean anomalies themselves (Fig. 2). Furthermore, the higher PCC values seen in the lower stratosphere are maintained for longer in RADINT. In CTRL, there is a sharp reduction around 80 hPa and below during the final warming period which recovers toward the summer as seen in previous sections. The upper stratosphere can be seen to show negative PCC which is expected because of the dependence of ozone production and loss cycles on temperature, with a higher temperature leading to less ozone production and more ozone loss (Randel 1993).

The SWT EFP in RADINT is especially strong above 30 hPa and peaks around the summer solstice. In the lower stratosphere, the SWT EFP in RADINT peaks earlier, since it reflects not just the magnitude of SWT but the correlation between SWT and T, which is dynamically controlled. SWT depends on ozone, and as can be seen from Fig. 8, the correlation between temperature and ozone drops around the final warming. The differences in LWT EFP are relatively minor throughout the domain. Overall, the ozone radiative feedback can be seen to reduce the net radiative damping throughout the domain.

c. *Final warming date*

We finally consider some diagnostics involving the FWD, using the widely used criterion defined in Black and McDaniel (2007): the date that the 50-hPa zonal-mean zonal wind at 60°S falls below 10 m s^{-1} based on 5-day averages. The climatological distributions of the FWDs in RADINT and in

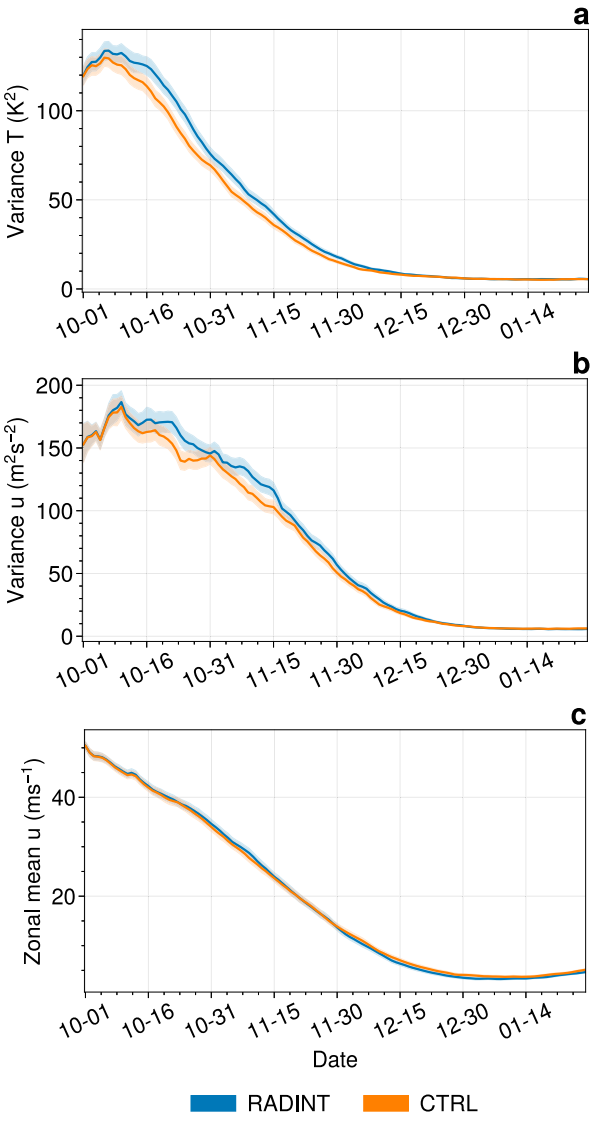

FIG. 10. (a),(b) The temperature (K^2) and zonal wind ($m^2\ s^{-2}$) variance about the zonal mean and (c) the zonal-mean zonal wind ($m\ s^{-1}$) for RADINT (blue) and CTRL (orange). The temperature variance is calculated at 60°S and 80 hPa and the wind at 60°S and 50 hPa.

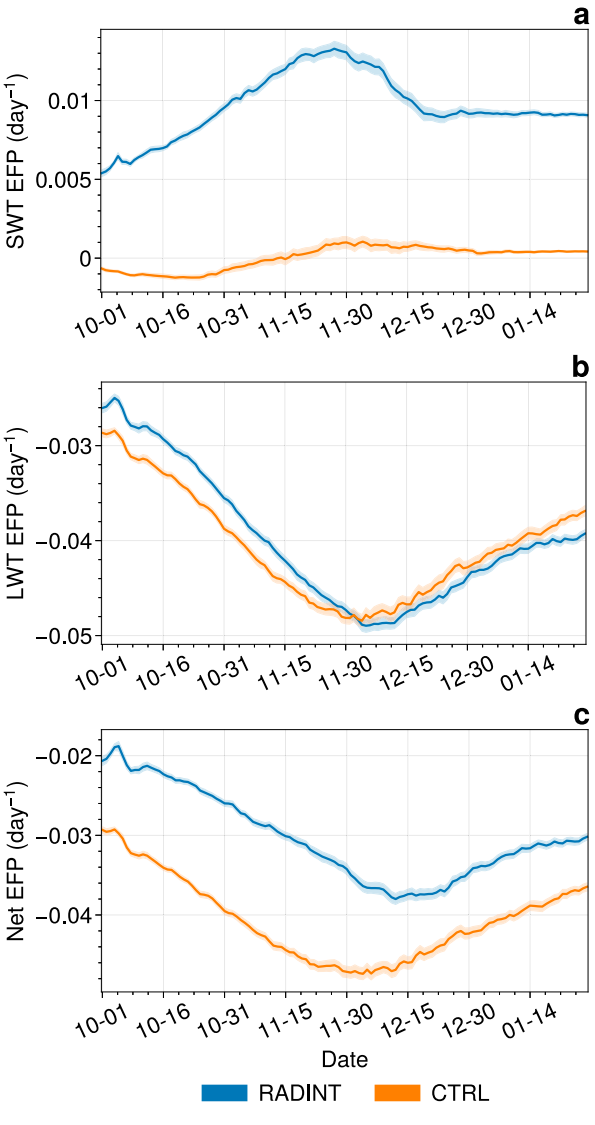

FIG. 11. EFP for SWT, LWT, and their sum (Net) all in units of per day for deviations away from the zonal mean. This is calculated at 60°S and 80 hPa.

CTRL are shown in Fig. 14. The mean FWD in RADINT is 8 December whereas that in CTRL is 9 December, a difference of only 1 day. Performing a two-sample t test gives a p value of 0.5 and a t-statistic of -0.7. Therefore, there is no statistically significant difference between the mean FWD in CTRL and RADINT. This is not unexpected given the very similar zonal-mean winds seen in Fig. 10c.

We now investigate whether there is a difference in the impact of interactive ozone on the waves between early and late FWD. The early and late groups were generated using the 20th and 80th quantiles on the FWDs. Using the two separate groups, the analysis performed in section 3b was repeated. Figure 15 shows the ozone–temperature PCC values for the early and late FWD groups for both RADINT and CTRL. As seen in Fig. 8, RADINT shows higher PCC values overall than CTRL. When comparing the early and late groups in RADINT and CTRL, a shift in the overall structure of the curves following the shift in the FWD is observed. This confirms that the dip in correlations in Fig. 8 is due to the timing of the vortex breakdown, rather than to the seasonality of the SWT. A similar shift in the structure of the EFP curves is also found (not shown). Note that the late group in both RADINT and CTRL is seen to have lower PCC values than the early group, suggesting different dynamical regimes for the two groups. However, investigation into this feature is outside the scope of this paper.

Figure 16 shows the time series of the distributions of the FWD across the RADINT and CTRL ensembles. The distributions

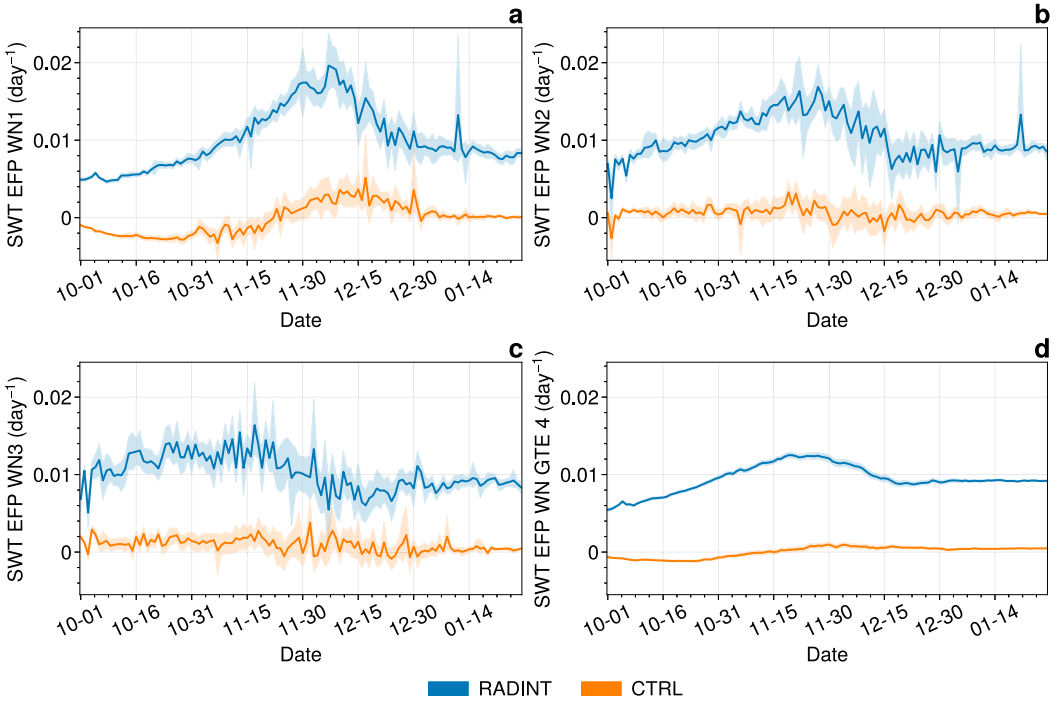

FIG. 12. EFP contributions for (a) zonal wavenumber 1, (b) zonal wavenumber 2, (c) zonal wavenumber 3, and (d) zonal wavenumbers greater than or equal to 4. As in the previous plots, this is calculated at 60°S and 80 hPa.

from the two model versions vary strongly and coherently from year to year, suggesting some interannual predictability of the FWD. We note in passing that both ensembles show fluctuations following an approximate 11-yr period which is in sync with the solar cycle, an interesting feature that we do not consider further. Figure 16 also shows that the observed FWDs (obtained from ERA5) lie within the interquartile range (IQR) of the yearly distributions approximately half of the time for both RADINT and

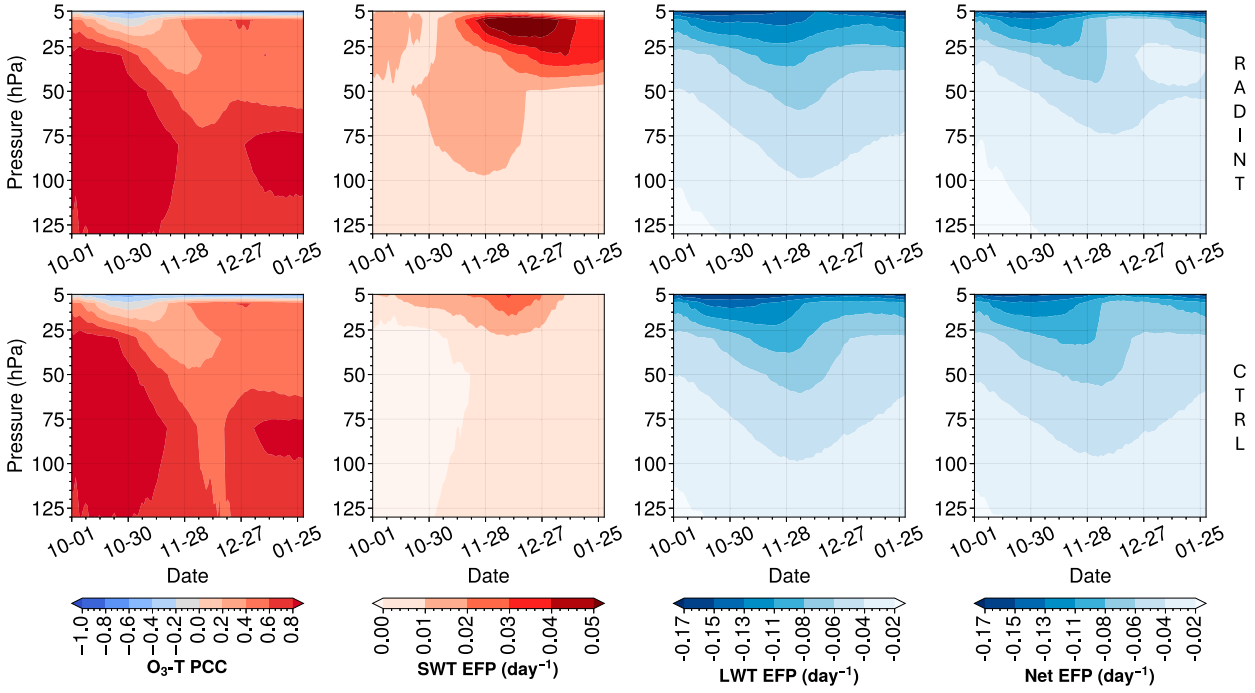

FIG. 13. (top) RADINT and (bottom) CTRL contour plots of the mean values of the (left to right) O_3–T correlations, SWT EFP, LWT EFP, and Net EFP given as a function of height and date.

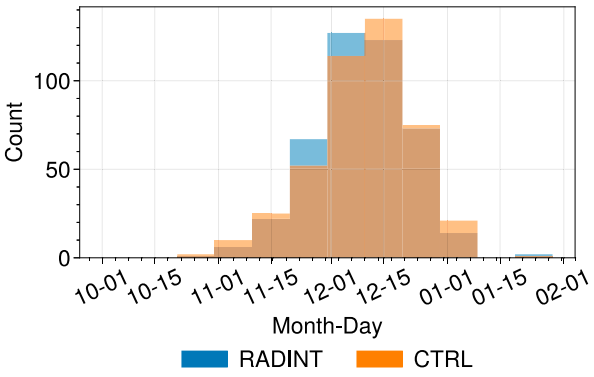

FIG. 14. Histogram of FWD for RADINT (blue) and CTRL (orange) across all years and ensemble members.

CTRL, indicating reliable forecasts for both experiments. We note that the ensemble spread of the FWD seems larger in CTRL than in RADINT, which is not consistent with the increased spread in zonal-mean variability we found in RADINT (Figs. 4 and 6). However, the small sample size of $n = 29$, we argue, is quite small to detect such a small change in variability. Given this small sample size, to evaluate the skill of the forecasted FWD, we restrict attention to simple deterministic metrics based on the ensemble-mean FWD for each year.

The most commonly used such metric is the anomaly correlation coefficient (ACC) between the ensemble-mean and reanalysis FWD across the different years. Scatterplots of those values are shown in Fig. 17 along with the ACC and its standard error, which confirm that there is skill in both the RADINT and CTRL forecasts. The ACC is found to be higher in CTRL than in RADINT, appearing to suggest that interactive ozone degrades forecast skill. This is not necessarily unexpected given that the model was tuned without interactive ozone. However, it also may reflect limitations in the ACC as a metric of forecast skill. Under the assumption that the predictable component of interannual variability is represented by the model ensemble mean (Kumar 2009), the strength of the forecast signal can be found by regressing the reanalysis FWD against the ensemble-mean FWD (see section 3.3 of Falkena et al. 2022). A perfect model would have a slope of unity; a slope greater than unity indicates that the signal strength in the model is too weak. The regression lines are plotted and their slopes with standard errors are recorded in Fig. 17. Although the uncertainties on these values are considerable given the limited sample size of the forecasts, CTRL shows a too-weak signal, which is increased in RADINT to a level more consistent with observations. This is consistent with the observation that in general the interannual variability of the SH polar cap temperature in the IFS has been shown to improve with interactive ozone using HLO, although is still too low in spring compared to ERA5 (personal correspondence, not shown).

In this respect, then, interactive ozone appears to improve the predictability of the FWD in the ECMWF model. The strengthening of the forecast signal is what can be expected from interactive ozone, as it provides a positive feedback on

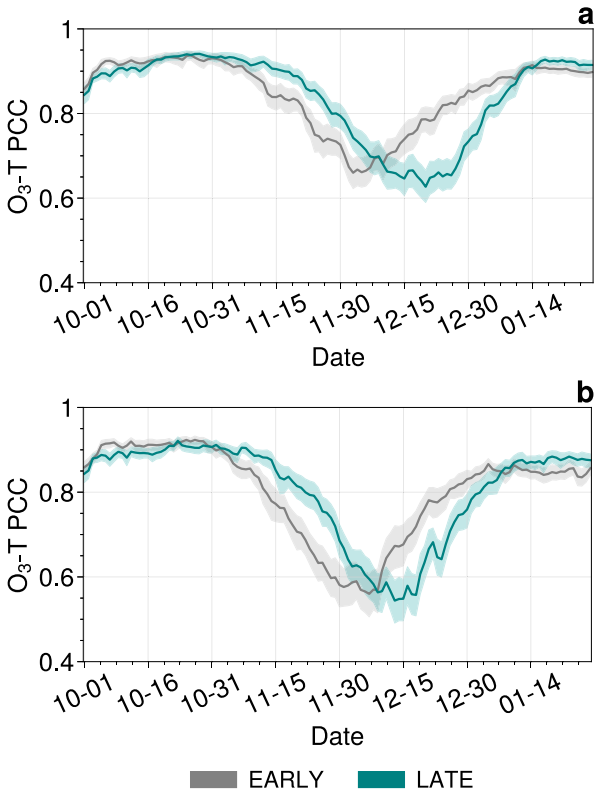

FIG. 15. PCC time series between ozone and temperature plotted for groups of late (green) and early (gray) FWD for (a) RADINT and (b) CTRL. As in section 3b, the calculation is performed for deviations from the zonal mean at 60°S and 80 hPa.

deviations from climatology. How can we then understand the decrease in the ACC? From Eq. (8) of Falkena et al. (2022), the ACC is proportional to the regression coefficient. Thus, all things being equal, a larger regression coefficient implies a larger ACC, even though a regression coefficient that is larger than unity implies a signal deficit. We suggest that in the presence of a signal deficit, the ACC may be a misleading measure of forecast skill.

4. Summary

This paper has quantified the effect of the ozone radiative feedback on stratospheric variability during the SH final warming period, as a first step in quantifying its role in tropospheric variability and predictability on S2S time scales. The ozone radiative feedback due to interactive ozone is quantified both on waves, i.e., deviations from the zonal mean, and on the zonal-mean variability itself, i.e., deviations from the ensemble mean, for both temperatures and zonal wind, using an ensemble seasonal hindcast system with and without interactive ozone. The strength of the feedback is quantified using an EFP. The work presented here thus distinguishes itself from previous research, which focused largely on the impact of interactive ozone on the zonal mean.

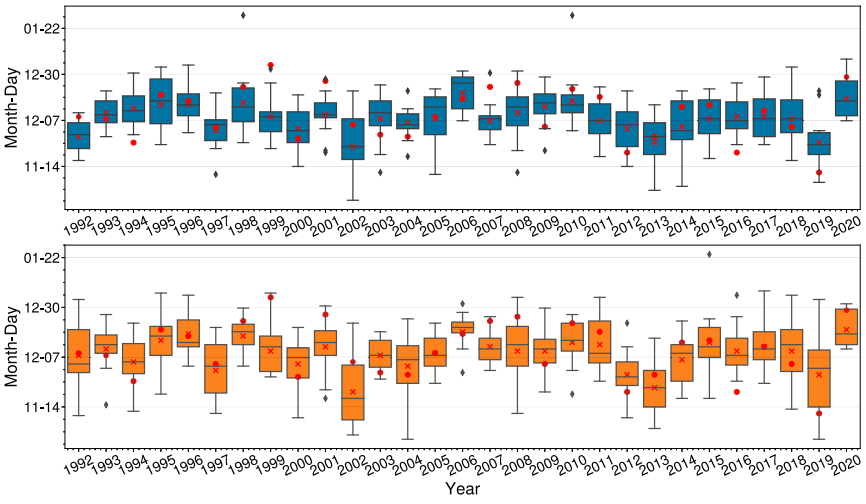

FIG. 16. Time series of the FWD for (top) RADINT and (bottom) CTRL. The boxplots show the IQR between the 15 ensemble members for a given year. The whiskers extend to the farthest data point within 1.5 times the IQR from the nearest hinge, and the diamonds represent the outliers. The ERA5 FWD is shown using a red circle marker, while the red cross shows the mean FWD across the ensemble for each experiment.

The use of hindcast ensembles initialized on 1 October and run for 4 months is motivated by experience from S2S prediction, which suggests significant predictability of the summertime SAM, and therefore surface conditions, arising from predictability of the stratospheric vortex evolution (Byrne et al. 2019; Lim et al. 2021). For the purpose of this study, the setup allows for a quantification of the effect of interactive ozone on SH high-latitude stratospheric variability during the vortex breakdown period, following the development of the ozone hole itself which is already well established by 1 October. While the ozone hole has been the main motivation for earlier studies of interactive ozone, the present setup is more relevant for S2S prediction. The large sample size from the hindcast ensembles allows the quantification to be performed as a function of day of year, in order to account for the strong nonstationarity of the stratosphere during this part of the seasonal cycle. The ensemble setup also avoids the potentially confounding influence of interannual variability on the statistics, which is difficult to quantify with only a limited number of years, in order to focus on the model spread for a given year.

We show that there is a radiative feedback acting both on the zonal mean and on the wave variability when including interactive ozone (RADINT), which strengthens the positive correlation between temperature and ozone in the polar lower stratosphere compared to not including interactive ozone (CTRL). The quantification of this feedback using the EFP diagnostic confirms the expectation that the primary effect of interactive ozone is through the shortwave radiation, which provides a positive feedback and thereby acts to

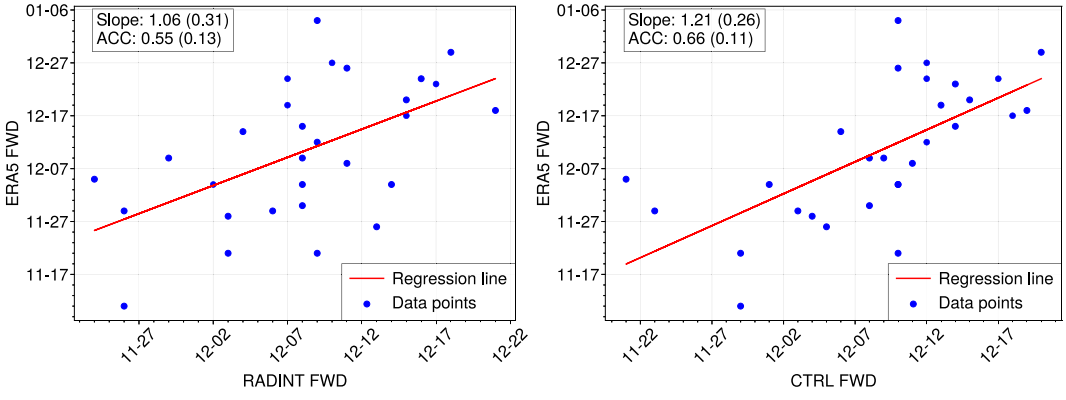

FIG. 17. ERA5 FWD regressed onto ensemble-mean FWDs of (left) RADINT and (right) CTRL, with the regression line shown in red and the data points shown in blue. The legend provides the values of the slope and the ACC along with the standard error in parentheses.

significantly reduce the net radiative damping (which is dominated by longwave radiative cooling) on both the zonal-mean variability and the waves (Figs. 5 and 11). The positive feedback from the shortwave EFP is found to have the largest impact on wavenumbers 1 and 2 just before the final warming, compared to all wavenumbers as a whole (Fig. 12). The feedback is shown to increase the variability in winds and temperatures in both the zonal mean and waves (Figs. 4, 6 and 10). In all the results, there is a seasonality (although stronger for the waves than for the zonal-mean variability) that is observed due to the return of sunlight to the poles and the subsequent vortex breakdown, and the relative differences between RADINT and CTRL EFP and variances are seen to maximize during this period. This importance of the vortex breakdown itself for the observed seasonality was confirmed by comparing late and early breakdowns (Fig. 15). Finally, the feedback was shown to amplify the predictable signal of the final warming date, bringing it more in line with what is expected from reanalysis (Fig. 17).

The findings of this study reveal the important effect of interactive ozone via shortwave radiation in increasing the variability of both waves and the zonal mean in the polar lower stratosphere during the SH final breakdown period. Based on previous literature, we can expect an effect on stratosphere–troposphere coupling. This possibility will be explored in future work.

Acknowledgments. Meryl C. Anil acknowledges funding from the University of Reading. We thank the reviewers for their constructive feedback which helped to improve the manuscript.

Data availability statement. The DOI for the data used in this paper are as follows. Experiment using interactive ozone (RADINT): https://doi.org/10.21957/975c-z032. Experiment using an ozone climatology (CTRL): https://doi.org/10.21957/s8r3-7v64.

APPENDIX

Brief Outline of the Hybrid Linear Ozone Scheme and Its Suitability for This Study

An outline of the HLO scheme is provided here. In brief, the scheme functions in the same way and with the same linearizations as the Cariolle–Déqué (CD) scheme but differs in how the coefficients are derived. Rather than taking all coefficients from a chemistry model simulation, coefficients are taken or derived from analyses where possible. The mean ozone climatology of the scheme is from the CAMS interim reanalysis (CAMSiRA; Flemming et al. 2017), the mean temperature climatology is from ERA5, and the mean net production rate of ozone is diagnosed by nudging the ozone field toward CAMSiRA values in an IFS run constrained by ERA5 winds, basically asking what the net effect of chemical processes must have been each time step, to have given the analyzed space–time evolution of the ozone field. A monthly climatology of the net ozone production rate is calculated. The linear perturbation sensitivities or rate coefficients used for HLO cannot be directly obtained from observational data, so are taken from the CD scheme, but importantly are modified where needed to ensure physical consistency with the diagnosed mean net production rates. The coefficients are calculated and adjusted based on the diagnosed tendencies of ozone chemistry in the period 2005–12 and are directly representative of ozone chemistry in this period. Given the observed and expected time evolution of ozone-depleting substances and stratospheric ozone, this is considered a good approximation from the 1990s to the present day. The version in this paper assumes that the drivers of stratospheric chemistry have a fixed seasonal cycle.

With these choices, and apart from nonlinearities in the chemistry, one might expect the mean climatological ozone produced by the HLO scheme to match the CAMSiRA ozone climatology, if the winds and temperature in the model run are consistent with ERA5 data. However, the mean ozone will differ from the CAMS climatology in the case that the model circulation or temperatures are biased, as they typically are in longer integrations, but this is how a perfect representation of the chemistry would also behave. Tests show that diagnosed HLO net ozone production is stable over time, and when HLO is used in a model with freely evolving ozone, it produces accurate ozone simulations in almost all situations. The climatological mean effect of heterogeneous chemistry is included in the model and is representative of chemistry occurring in the presence of near present-day concentrations of ozone-depleting substances.

Since the main limitation of HLO is its limited ability to represent the interannual variability of heterogeneous ozone chemistry around Antarctica, which has significant nonlinearities and dependence on reservoir species, we further emphasize its suitability for our study here. We show some plots of ozone in Fig. A1 produced by a model integration using HLO (top row) compared to the ERA5 reanalysis (bottom row). The model integration was initialized on 1 January, and although the model physics and ozone chemistry were running freely from that date, the winds were nudged to ERA5 values to keep the synoptic variability close to the reanalysis. There are some obvious differences between reanalysis ozone and HLO, the reanalysis has more fine structure, as expected from its higher resolution (TL639 vs TL255 for the nudged run, which nudges spatial scales only up to T63), and the ozone hole is slightly deeper in the reanalysis, which is probably related to the limitations of the linear ozone scheme. Nonetheless, the synoptic-scale variability of the ozone field in both space and time is represented remarkably well by HLO. The patterns of ozone variability in the free-running model are thus expected to be realistic, at least to the extent that the dynamic variability is realistic. We thus consider HLO to be fully suited for the purposes of this study.

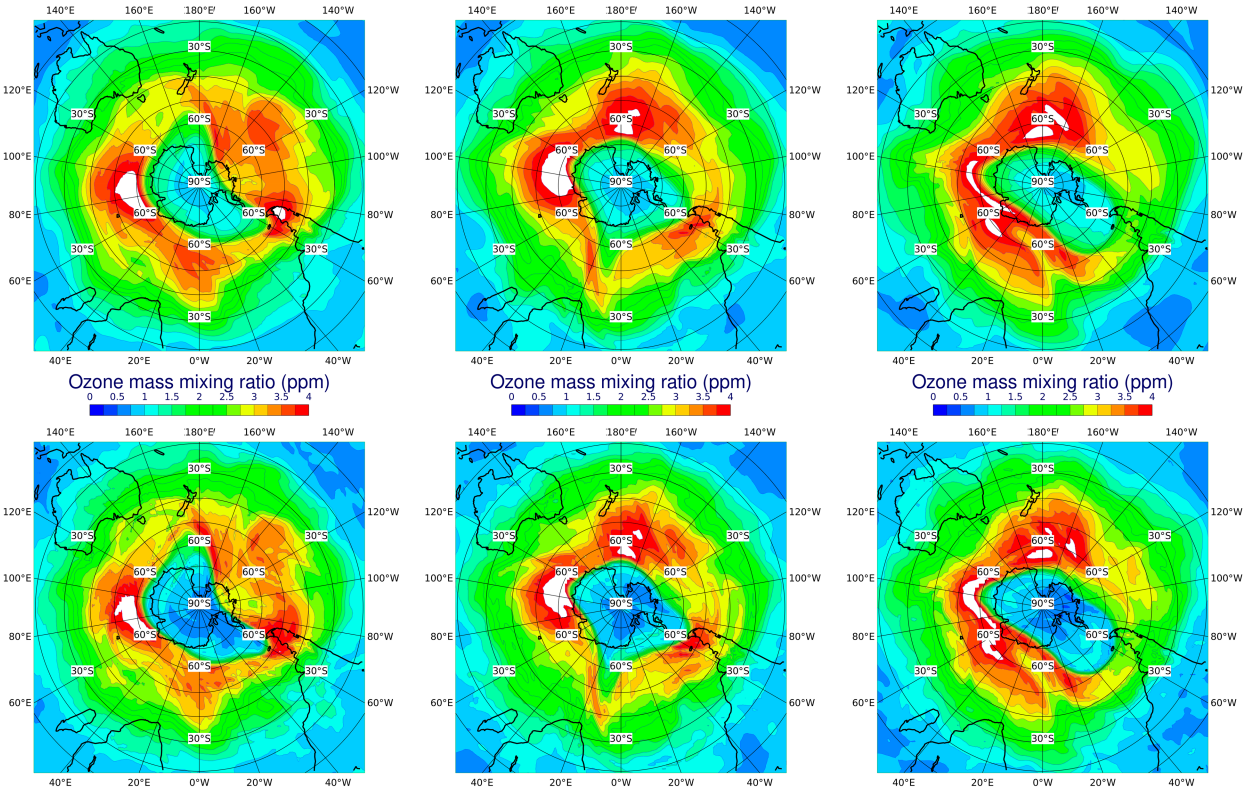

FIG. A1. Instantaneous values of ozone at 70 hPa at 0000 UTC (left) 6, (middle) 9, and (right) 12 Nov 2009 from an 11-month integration with (top) free-running ozone calculated from HLO and winds nudged to ERA5 and (bottom) ozone calculated from the ERA5 reanalysis.

REFERENCES

Albers, J. R., J. P. McCormack, and T. R. Nathan, 2013: Stratospheric ozone and the morphology of the Northern Hemisphere planetary waveguide. *J. Geophys. Res. Atmos.*, **118**, 563–576, https://doi.org/10.1029/2012JD017937.

Baldwin, M. P., and T. J. Dunkerton, 2001: Stratospheric harbingers of anomalous weather regimes. *Science*, **294**, 581–584, https://doi.org/10.1126/science.1063315.

Bergner, N., M. Friedel, D. I. V. Domeisen, D. Waugh, and G. Chiodo, 2022: Exploring the link between austral stratospheric polar vortex anomalies and surface climate in chemistry-climate models. *Atmos. Chem. Phys.*, **22**, 13 915–13 934, https://doi.org/10.5194/acp-22-13915-2022.

Black, R. X., and B. A. McDaniel, 2007: Interannual variability in the Southern Hemisphere circulation organized by stratospheric final warming events. *J. Atmos. Sci.*, **64**, 2968–2974, https://doi.org/10.1175/JAS3979.1.

Byrne, N. J., T. G. Shepherd, T. Woollings, and R. A. Plumb, 2017: Nonstationarity in Southern Hemisphere climate variability associated with the seasonal breakdown of the stratospheric polar vortex. *J. Climate*, **30**, 7125–7139, https://doi.org/10.1175/JCLI-D-17-0097.1.

——, and ——, 2018: Seasonal persistence of circulation anomalies in the Southern Hemisphere stratosphere and its implications for the troposphere. *J. Climate*, **31**, 3467–3483, https://doi.org/10.1175/JCLI-D-17-0557.1.

——, ——, and I. Polichtchouk, 2019: Subseasonal-to-seasonal predictability of the Southern Hemisphere eddy-driven jet during austral spring and early summer. *J. Geophys. Res. Atmos.*, **124**, 6841–6855, https://doi.org/10.1029/2018JD030173.

Cariolle, D., and M. Déqué, 1986: Southern Hemisphere medium-scale waves and total ozone disturbances in a spectral general circulation model. *J. Geophys. Res.*, **91**, 10 825–10 846, https://doi.org/10.1029/JD091iD10p10825.

ECMWF, 2020: IFS Documentation. CY47R1, ECMWF, 822 pp., https://www.ecmwf.int/en/publications/ifs-documentation.

Falkena, S. K. J., J. de Wiljes, A. Weisheimer, and T. G. Shepherd, 2022: Detection of interannual ensemble forecast signals over the North Atlantic and Europe using atmospheric circulation regimes. *Quart. J. Roy. Meteor. Soc.*, **148**, 434–453, https://doi.org/10.1002/qj.4213.

Flemming, J., and Coauthors, 2017: The CAMS interim reanalysis of carbon monoxide, ozone and aerosol for 2003–2015. *Atmos. Chem. Phys.*, **17**, 1945–1983, https://doi.org/10.5194/acp-17-1945-2017.

Fogt, R. L., and G. J. Marshall, 2020: The Southern Annular Mode: Variability, trends, and climate impacts across the Southern Hemisphere. *Wiley Interdiscip. Rev.: Climate Change*, **11**, e652, https://doi.org/10.1002/wcc.652.

Friedel, M., G. Chiodo, A. Stenke, D. I. V. Domeisen, and T. Peter, 2022: Effects of Arctic ozone on the stratospheric spring onset and its surface impact. *Atmos. Chem. Phys.*, **22**, 13 997–14 017, https://doi.org/10.5194/acp-22-13997-2022.

Gerber, E. P., and Coauthors, 2010: Stratosphere-troposphere coupling and annular mode variability in chemistry-climate models. *J. Geophys. Res.*, **115**, D00M06, https://doi.org/10.1029/2009JD013770.

Gillett, N. P., J. F. Scinocca, D. A. Plummer, and M. C. Reader, 2009: Sensitivity of climate to dynamically-consistent zonal asymmetries in ozone. *Geophys. Res. Lett.*, **36**, L10809, https://doi.org/10.1029/2009GL037246.

Haase, S., and K. Matthes, 2019: The importance of interactive chemistry for stratosphere–troposphere coupling. *Atmos. Chem. Phys.*, **19**, 3417–3432, https://doi.org/10.5194/acp-19-3417-2019.

Hendon, H. H., E.-P. Lim, and S. Abhik, 2020: Impact of interannual ozone variations on the downward coupling of the 2002 Southern Hemisphere stratospheric warming. *J. Geophys. Res. Atmos.*, **125**, e2020JD032952, https://doi.org/10.1029/2020JD032952.

Hitchcock, P., T. G. Shepherd, and S. Yoden, 2010: On the approximation of local and linear radiative damping in the middle atmosphere. *J. Atmos. Sci.*, **67**, 2070–2085, https://doi.org/10.1175/2009JAS3286.1.

Jucker, M., and R. Goyal, 2022: Ozone-forced Southern Annular Mode during Antarctic stratospheric warming events. *Geophys. Res. Lett.*, **49**, e2021GL095270, https://doi.org/10.1029/2021GL095270.

Kang, S. M., L. M. Polvani, J. C. Fyfe, and M. Sigmond, 2011: Impact of polar ozone depletion on subtropical precipitation. *Science*, **332**, 951–954, https://doi.org/10.1126/science.1202131.

Kumar, A., 2009: Finite samples and uncertainty estimates for skill measures for seasonal prediction. *Mon. Wea. Rev.*, **137**, 2622–2631, https://doi.org/10.1175/2009MWR2814.1.

Lim, E.-P., and Coauthors, 2021: The 2019 Southern Hemisphere stratospheric polar vortex weakening and its impacts. *Bull. Amer. Meteor. Soc.*, **102**, E1150–E1171, https://doi.org/10.1175/BAMS-D-20-0112.1.

McLandress, C., 2002: The seasonal variation of the propagating diurnal tide in the mesosphere and lower thermosphere. Part I: The role of gravity waves and planetary waves. *J. Atmos. Sci.*, **59**, 893–906, https://doi.org/10.1175/1520-0469(2002)059<0893:TSVOTP>2.0.CO;2.

——, T. G. Shepherd, J. F. Scinocca, D. A. Plummer, M. Sigmond, A. I. Jonsson, and M. C. Reader, 2011: Separating the dynamical effects of climate change and ozone depletion. Part II: Southern Hemisphere troposphere. *J. Climate*, **24**, 1850–1868, https://doi.org/10.1175/2010JCLI3958.1.

Monge-Sanz, B. M., and Coauthors, 2022: A stratospheric prognostic ozone for seamless Earth system models: performance, impacts and future. *Atmos. Chem. Phys.*, **22**, 4277–4302, https://doi.org/10.5194/acp-22-4277-2022.

Nathan, T. R., and E. C. Cordero, 2007: An ozone-modified refractive index for vertically propagating planetary waves. *J. Geophys. Res.*, **112**, D02105, https://doi.org/10.1029/2006JD007357.

Oehrlein, J., G. Chiodo, and L. M. Polvani, 2020: The effect of interactive ozone chemistry on weak and strong stratospheric polar vortex events. *Atmos. Chem. Phys.*, **20**, 10 531–10 544, https://doi.org/10.5194/acp-20-10531-2020.

Oh, J., S.-W. Son, J. Choi, E.-P. Lim, C. Garfinkel, H. Hendon, Y. Kim, and H.-S. Kang, 2022: Impact of stratospheric ozone on the subseasonal prediction in the Southern Hemisphere spring. *Prog. Earth Planet. Sci.*, **9**, 25, https://doi.org/10.1186/s40645-022-00485-4.

Polvani, L. M., D. W. Waugh, G. J. P. Correa, and S.-W. Son, 2011: Stratospheric ozone depletion: The main driver of twentieth-century atmospheric circulation changes in the Southern Hemisphere. *J. Climate*, **24**, 795–812, https://doi.org/10.1175/2010JCLI3772.1.

Rae, C. D., J. Keeble, P. Hitchcock, and J. A. Pyle, 2019: Prescribing zonally asymmetric ozone climatologies in climate models: Performance compared to a chemistry-climate model. *J. Adv. Model. Earth Syst.*, **11**, 918–933, https://doi.org/10.1029/2018MS001478.

Randel, W. J., 1993: Global normal-mode Rossby waves observed in stratospheric ozone data. *J. Atmos. Sci.*, **50**, 406–420, https://doi.org/10.1175/1520-0469(1993)050<0406:GNMRWO>2.0.CO;2.

——, and F. Wu, 1999: Cooling of the Arctic and Antarctic polar stratospheres due to ozone depletion. *J. Climate*, **12**, 1467–1479, https://doi.org/10.1175/1520-0442(1999)012<1467:COTAAA>2.0.CO;2.

Rieder, H. E., G. Chiodo, J. Fritzer, C. Wienerroither, and L. M. Polvani, 2019: Is interactive ozone chemistry important to represent polar cap stratospheric temperature variability in Earth-System Models? *Environ. Res. Lett.*, **14**, 044026, https://doi.org/10.1088/1748-9326/ab07ff.

Saggioro, E., and T. G. Shepherd, 2019: Quantifying the timescale and strength of Southern Hemisphere intraseasonal stratosphere-troposphere coupling. *Geophys. Res. Lett.*, **46**, 13479–13487, https://doi.org/10.1029/2019GL084763.

Salby, M. L., E. A. Titova, and L. Deschamps, 2012: Changes of the Antarctic ozone hole: Controlling mechanisms, seasonal predictability, and evolution. *J. Geophys. Res.*, **117**, D10111, https://doi.org/10.1029/2011JD016285.

Silverman, V., N. Harnik, K. Matthes, S. W. Lubis, and S. Wahl, 2018: Radiative effects of ozone waves on the Northern Hemisphere polar vortex and its modulation by the QBO. *Atmos. Chem. Phys.*, **18**, 6637–6659, https://doi.org/10.5194/acp-18-6637-2018.

Son, S.-W., A. Purich, H. H. Hendon, B.-M. Kim, and L. M. Polvani, 2013: Improved seasonal forecast using ozone hole variability? *Geophys. Res. Lett.*, **40**, 6231–6235, https://doi.org/10.1002/2013GL057731.

Thompson, D. W. J., and J. M. Wallace, 2000: Annular modes in the extratropical circulation. Part I: Month-to-month variability. *J. Climate*, **13**, 1000–1016, https://doi.org/10.1175/1520-0442(2000)013<1000:AMITEC>2.0.CO;2.

Yook, S., D. W. J. Thompson, S. Solomon, and S.-Y. Kim, 2020: The key role of coupled chemistry–climate interactions in tropical stratospheric temperature variability. *J. Climate*, **33**, 7619–7629, https://doi.org/10.1175/JCLI-D-20-0071.1.

Young, P. J., and Coauthors, 2018: Tropospheric Ozone Assessment Report: Assessment of global-scale model performance for global and regional ozone distributions, variability, and trends. *Elementa*, **6**, 10, https://doi.org/10.1525/elementa.265.